4-ft parachute are somewhat higher than those of the small models. The higher drag coefficients may be caused by a difference in form which presently cannot be explained. Also, the projected diameter of the 4-ft parachute was larger than expected. This may have been caused by the elasticity of the cloth and lines or through the rather loose line connections. The drag coefficients are in all cases based on the design diameter.

In spite of the differences of drag coefficients, the fact that the parachute that was 12 times larger, with a Reynolds number about 15 times as high, functioned essentially as the prototype models, may be taken as proof of the validity of the basic concept and of the value of experiments with small parachute models.

In summary, a 4-ft supersonic guide surface parachute, based on information obtained from model tests, has worked very well. However, the presented information should be considered merely as design guide lines. A parachute for supersonic application should undergo specific wind-tunnel tests under consideration of the operational conditions such as Mach number, Reynolds number, and forebody wake.

References

[1] Meyer, R. A., "Wind tunnel investigation of conventional types of parachute canopies in supersonic flow," Wright Air Development Center Tech. Rept. 58-532 (1958).

[2] Connors, J. F. and Lovell, J. C., "Some observations on supersonic stabilization and deceleration devices," IAS Paper 60-19 (1960).

[3] Maynard, J. D., "Aerodynamic characteristics of parachutes at Mach numbers from 1.6 to 3.0," NASA Langley Research Center, Langley Field, Va., TN D-752 (1961).

[4] Heinrich, H. G., Rose, R. E., and Kovacevic, N. D., "Flow characteristics of rigid ribbon parachute canopies in supersonic flow," Air Force Flight Development Lab. Tech. Rept. AFFDL-TR-65-103 (1965).

[5] Engstrom, B. A., "Performance of trailing aerodynamic decelerators at high dynamic pressures," Wright Air Development Center Tech. Rept. 58-284, Pts. I–III (1960).

[6] Simms, L. W., "Evolution of the hyperflo parachute," *Transactions of the Eighth Symposium on Ballistic Missile and Space Technology* (Air Force Systems Command and Aerospace Corp., Los Angeles, Calif., 1963), Vol. II.

[7] Preiswerk, E., "Applications of the methods of gas dynamics to water flows with free surfaces," NACA TN 934 and TN 935 (1940).

[8] Heinrich, H. G., "Aerodynamic characteristics of the supersonic guide surface parachute and the spiked ribbon parachutes," Air Force Flight Development Lab. Tech. Rept. AFFDL-TR-65-104 (1965).

[9] Bailey, R. O., "Analytical and experimental investigation of sensitivity to Mach number of the mass flow and flow field properties of the supersonic guide surface parachute," Master Thesis, Univ. of Minnesota, Minneapolis, Minn. (October 1963).

[10] Lowry, J. F., "Aerodynamic characteristics of various types of full scale parachutes at Mach numbers from 1.8 to 3.0," Arnold Engineering Development Center Tech. Rept. AEDC-TDR-64-120 (1964).

MARCH-APRIL 1966 J. AIRCRAFT VOL. 3, NO. 2

Beneficial Interference Effects Obtained with Ring Wings at Supersonic Speeds

ARNOLD R. JOHNSON,* HAROLD R. MEAD,† AND RICHARD A. SCHEUING‡
Grumman Aircraft Engineering Corporation, Bethpage, N. Y.

An investigation of the use of ring wings to develop beneficial aerodynamic interference effects at supersonic speeds is described. Consideration is given to both symmetrical and unsymmetrical configurations having conical noses and conical boattails. Experimental results for Mach numbers of 1.9 to 2.9 demonstrate that very significant drag reductions can be obtained even with simplified ring-wing-body combinations. By the addition of a ring to a symmetrical boattailed body, reductions as high as 40% in total drag and 88% in wave drag were measured. These beneficial interference effects are reduced by deviation from the design Mach number or from zero angle of attack. Significant interference lift, not strongly affected by change in Mach number, was obtained with the unsymmetrical models, which accounted for their developing higher L/D's than the symmetrical models. However, since no attempt was made to optimize either type of configuration with regard to L/D, the test values may not be representative of those obtainable. The experimental results are shown to compare favorably with the pressure distributions and optimum configuration geometry calculated by a simplified analytical method.

Introduction

THE unique geometry of the ring wing presents an ideal mechanism through which large beneficial aerodynamic effects can be generated at supersonic speeds. Significant wave drag reduction is obtained when the ring wing is employed to reflect the high pressure field from the nose onto a boattail portion of the central body. If a partial ring wing is used, a substantial lift increment can be developed as the result of the interaction of the body nose pressure field on the wing. A number of theoretical investigations have shown that ring wings can be combined with slender bodies of revolution to produce configurations with near zero or zero wave drag at supersonic speeds. For example, Ferri[1] applied the method of characteristics to this problem, whereas Graham,[2] and others,[3,4] employed linearized theory. The large chord ring wings that are required for these zero wave

Received December 30, 1964; revision received September 17, 1965. The research effort described here was partially supported by the Office of Naval Research, Department of the Navy, under Contract Nonr 2922(00).

* Research Engineer.

† Head, Aerodynamics Research Group. Member AIAA.

‡ Assistant Chief of Research. Associate Fellow Member AIAA

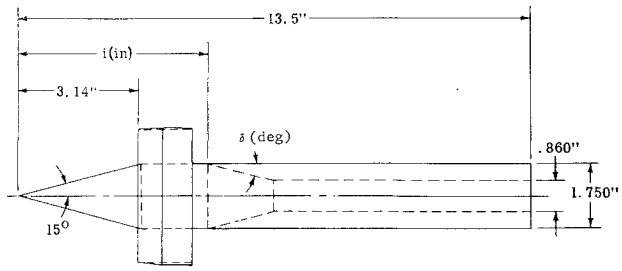

Fig. 1 Typical symmetrical ring-wing configurations.

drag configurations problably would have prohibitively large friction drags, as pointed out by some of these investigators.

Recognition of the natural objection to very large ring wing chords, plus a frequent requirement of specified base area, has led to a relaxation of the aim of complete wave drag cancellation. This approach was followed by Broglio,[5] wherein, using the method of characteristics, configurations were designed for use at a particular supersonic Mach number and zero angle of attack. Limited experimental results supported the theoretical conclusions that the wing-body combinations would have considerably less drag than the body alone at design conditions.

The present investigation, adopting the approach of partial wave drag cancellation, is concerned primarily with the experimental investigation of simple ring-wing configurations having conical noses, cylindrical inner wing surfaces, and conical boattails of given base area. The experimental program had several purposes: to obtain experimental evidence demonstrating that large wave drag reductions are possible with relatively unsophisticated symmetrical ring-wing configurations; to evaluate in a limited fashion the merits of unsymmetrical shapes; and to explore the off-design performance of both symmetrical and unsymmetrical configurations.

Supporting analytical work is presented in Ref. 6. It involves a reasonably straightforward, semiempirical procedure for predicting pressure distributions and for determining the location and angle of the boattail which produce maximum drag reduction for the class of configurations considered. Some comparisons with experimental results appear in the Appendix.

Experimental Program: General Remarks

The experimental program was conducted in the David Taylor Model Basin 18 × 18 in. supersonic wind tunnel. The specific test programs are outlined in Ref. 7. Axial force, normal force, pitching moment measurements, and extensive pressure surveys were taken at Mach numbers of 1.88, 2.15, 2.48, and 2.87 (the maximum available) at average Reynolds numbers per inch of 3.23×10^5, 2.75×10^5, 2.29×10^5, and 1.77×10^5, respectively. In the design of the models, 2.48 was chosen as the design Mach number so that data could be obtained at both an upper and lower off-design Mach number. In the computing of the force coefficients, the base drag was subtracted from the axial force. The reference area for the force coefficients was the maximum body cross-sectional area of the particular configuration.

A large portion of the pressure and force data acquired during this program is not contained in this paper but can be found in Ref. 6. This additional information generally supports the main conclusions and results given here, differing essentially in a quantitative sense only. Therefore, only the pertinent results for representative symmetrical and unsymmetrical configurations are presented here.

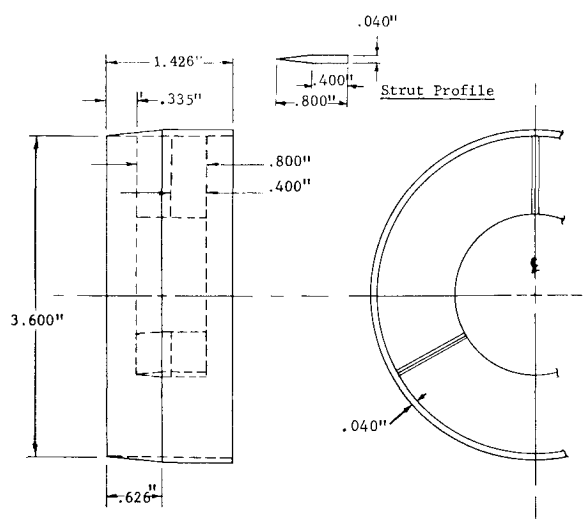

Fig. 2 Symmetrical ring wing.

Symmetrical Configurations: Experiments and Results

Description of Models

The basic symmetrical body is a cone-cylinder with a 15° semicone angle, as shown in Fig. 1 together with typical boattailed ring-wing configuration. In this figure, δ refers to the angle of the conical boattail in degrees, and i is the distance in inches from the body nose to the shoulder of the boattail. The long cylindrical afterbody is designed to isolate the boattail from disturbances, generated by the sting and balance windshield, which might be propagated upstream. The principal conical boattails tested had angles of 10°, 12°, 13°, 15°, and 20°. The wing shown in Fig. 2 has a profile with a flat inner surface and a half-wedge forward section followed by a constant thickness, blunt trailing-edge after-section. The wing, located 3.14 in. aft of the body nose, is supported by three struts of 5% thickness ratio, having a symmetrical wedge forward section and constant thickness after-section.

Zero-Lift Drag Reduction

An effort was made to determine experimentally the boattail angle and location that would provide the lowest zero-lift drag, C_{D_0}, at a Mach number of 2.48. The results are shown in Fig. 3 and indicate that the minimum-drag configuration has a 13.4° boattail located 4.91 in. aft of the nose. The value of C_{D_0} for this minimum-drag geometry is seen to be 0.201, which is 33% less than the experimental value of 0.298 for the

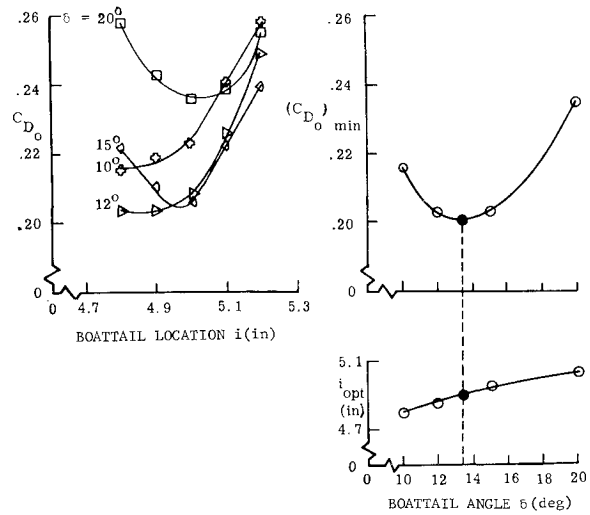

Fig. 3 Experimental determination of the minimum-drag symmetrical configuration at $M_\infty = 2.48$.

drag coefficient of the corresponding boattailed body alone. Furthermore, the minimum-drag configuration has a C_{D_0} which is 46% less than the experimental value of 0.373 for the drag of the nonboattailed wing-body combination.

It is interesting to consider the wave drag reduction associated with the addition of the wing to the boattailed body; this can be determined in an approximate fashion. The nonboattailed body is a cone-cylinder, and the wave drag coefficient of this configuration is equal to the pressure coefficient on the surface of the 15° cone (0.183) which is readily available from standard cone tables. Subtracting this value from the total drag coefficient of the body (0.243) and multiplying the result by the ratio of the wetted area of the boattailed body to that of the nonboattailed body, we obtain a rough estimate of the friction drag coefficient (0.041) for the boattailed body. It follows directly from the experimental drag coefficient of the boattailed body that its wave drag coefficient is approximately 0.257. The wave drag of the boattailed body in the presence of the wing is approximated by subtracting the total drag of the wing-plus-struts and the friction drag of the boattailed body from the total drag of the boattailed wing-body combination. The wing-plus-strut total drag (friction drag, wave drag, and interference of body nose on struts) is obtained as 0.130 by subtracting the drag of the nonboattailed body from that of the nonboattailed wing-body configuration. According to this method of estimating, then, we find that the favorable interference reduces the boattailed body wave drag from 0.257 to 0.030, which is approximately 88%.

Drag at Angle of Attack

One purpose of this investigation was to measure the influence of angle of attack on the drag characteristics of a configuration having large beneficial interference at zero lift. Because the configuration tested in this part of the investigation had to be selected on the basis of raw wind-tunnel data, it is slightly different from the minimum-drag geometry. Thus, whereas the experimentally determined minimum-drag symmetrical configuration had a 13.4° boattail 4.91 in. aft of the body nose, the model actually tested had a 13° boattail 4.95 in. aft of the body nose. Unless otherwise noted, all further force data for the symmetrical model refer to the latter configuration.

The variation of drag coefficient with angle of attack at Mach 2.48 for the symmetrical configuration is shown in Fig. 4. Corresponding boattailed body alone data have been added to this figure for comparative purposes. It can be seen that the beneficial interference effects decrease gradually as the angle of attack is increased. The winged configuration, for example, has the same drag coefficient at 5.5° angle of attack as the body alone has under zero-lift conditions, whereas both have the same drag coefficient at 6.9°. The lift produced by the wing is thus provided at no penalty in drag up to an angle of attack of 6.9°, with the result that lift-to-drag ratios in this range are increased significantly. The maximum L/D values occur at relatively low values of C_L.

Subsidiary Experiments

The basic wing of Fig. 2 was modified so that it would accept extensions to its chord. One of these was an internal wedge that tapers the inside wing surface to a sharp trailing edge; the other was a constant thickness, blunt base extension for use as a reference. Each adds 0.4 in. to the basic wing chord.

Both extensions were tested in combination with the basic nonboattailed body, and the configuration with the internal wedge extension showed definite merit.[6] This nonboattailed configuration exhibits approximately 3% less drag than the shorter chord basic wing configuration and 10% less than the constant thickness, extended chord reference wing.

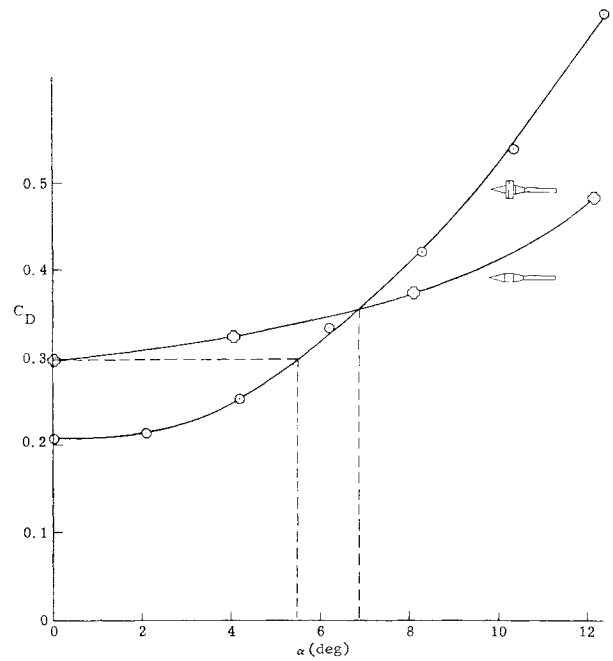

Fig. 4 Drag variation of the symmetrical configuration with angle of attack at $M_\infty = 2.48$.

This reduced level of drag is apparently a beneficial result of the positive pressure field generated by the body nose acting on the internal wedge section of the wing.

The internal wedge extended wing, used in combination with a body having a 13° boattail located 4.85 in. aft of the nose, proved superior to all of the other symmetrical configurations investigated during the course of this program. It has 10% less drag at zero lift than the basic configuration with boattailed body and 40% less drag than the boattailed body alone. This occurs in spite of the fact that the extended wing has a greater wetted area than the basic wing.

Unsymmetrical Configurations: Experiments and Results

Of the half- and third-ring-wing configurations tested, we have chosen to present data only for the former. The basic half body was designed originally to have the same volume and cross-sectional area distribution as the symmetrical cone-cylinder body of the full ring tests. The resulting nose angle of the half body is 20.74°. A modified version of the basic half body, having rounded corners, proved to be slightly superior aerodynamically and therefore was selected to be the one used in combination with the half wing. It has 98% of the volume of the basic body. As shown in Fig. 5, the half ring wing has a chord of 1.929 in., a radius of 2.29 in., and is located 3.35 in. aft of the nose. It has the same wing-plus-strut wetted area as the basic symmetrical wing. Only two

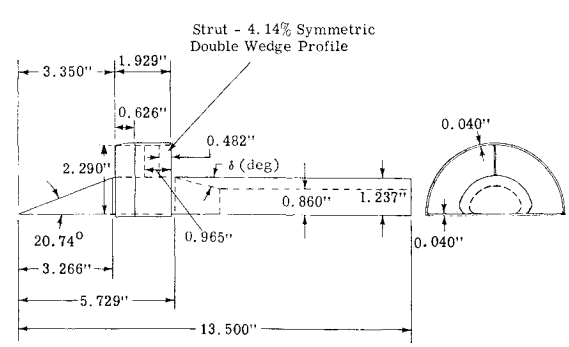

Fig. 5 Half-ring-wing configuration.

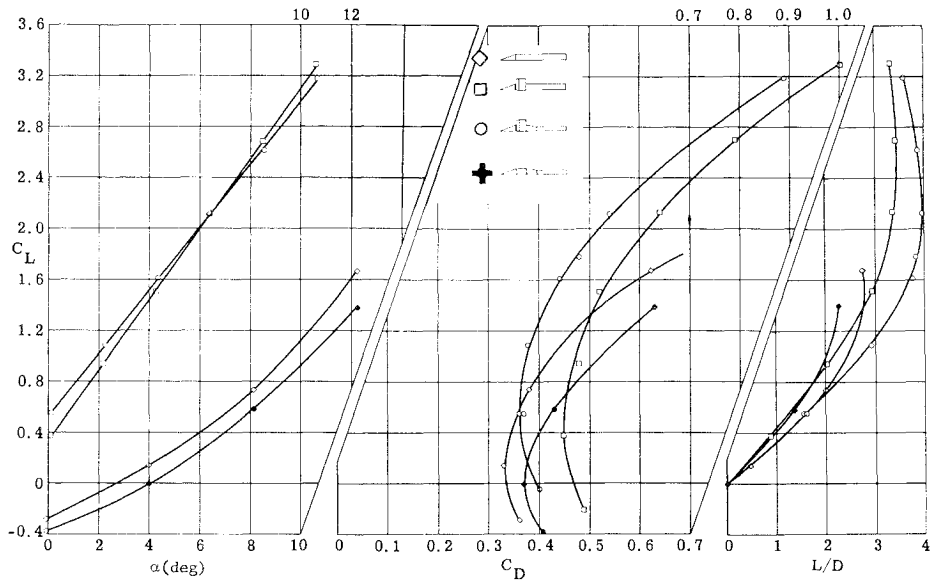

Fig. 6 Force characteristics of several half-model configurations at $M_\infty = 2.48$ showing the effects of the 12° boattail.

conical boattails (6.5° and 12°) were tested in this case so that a minimum-drag geometry could not be determined. A comparison of force data for the nonboattailed and the 12° boattailed half-wing configuration is shown in Fig. 6. Body alone data also have been added to this figure for reference.

The nonboattailed half body has a significant negative lift at zero angle of attack, but the addition of the half ring to this body introduces a large interference lift so that the wing-body combination exhibits a substantial positive lift at zero angle of attack. Boattailing the half body causes a significant increase in body drag and a large decrease in body lift. In spite of this decrease in performance of the body alone, the addition of the half wing to the boattailed body results in a minimum drag that is 20% lower than that of the nonboattailed wing-body combination, and a lift at zero angle of attack that is 50% higher. The latter effect is due primarily to the fact that the negative lift induced on the body by reflected wing pressures is diminished because boattailing has reduced the projected planform area of the body.

As mentioned, all of the force data presented here have had the wind-tunnel base drag subtracted. It should be noted that the base drag subtracted from the nonboattailed model is much larger than that subtracted from the boattailed configuration, primarily because of the large difference in base areas. Thus, the data that are presented here, with the base drag subtracted, favor the nonboattailed configuration. A fairer comparison might be obtained by considering an appropriate base drag for each configuration.

Comparison of Force Results of Symmetrical and Unsymmetrical Configurations

The boattailed symmetrical configuration is compared with the boattailed unsymmetrical configuration at $M_\infty = 2.48$ in Fig. 7. Both configurations have the same wing-plus-strut wetted areas, and the basic nonboattailed bodies have almost the same volume and cross-sectional area distribution. The maintenance of equivalent cross-sectional area distribution for the unsymmetrical body produces a large surface area and a nose of large cone angle. Both of these geometrical characteristics generally lead to a higher drag level for the unsymmetrical configuation. The results for the extended wing model with the internal wedge trailing edge are included for reference in Fig. 7 and are shown as dashed lines.

It should be noted that the body cross-sectional area aft of the boattail is considerably smaller for the symmetrical models than for the unsymmetric. This is due to sting mounting problems, which established the minimum base area of the half-body. Because of their larger boattail projected area (in the axial direction), the symmetrical configurations have a greater potential for the generation of interference thrust. Therefore, it is not too surprising that

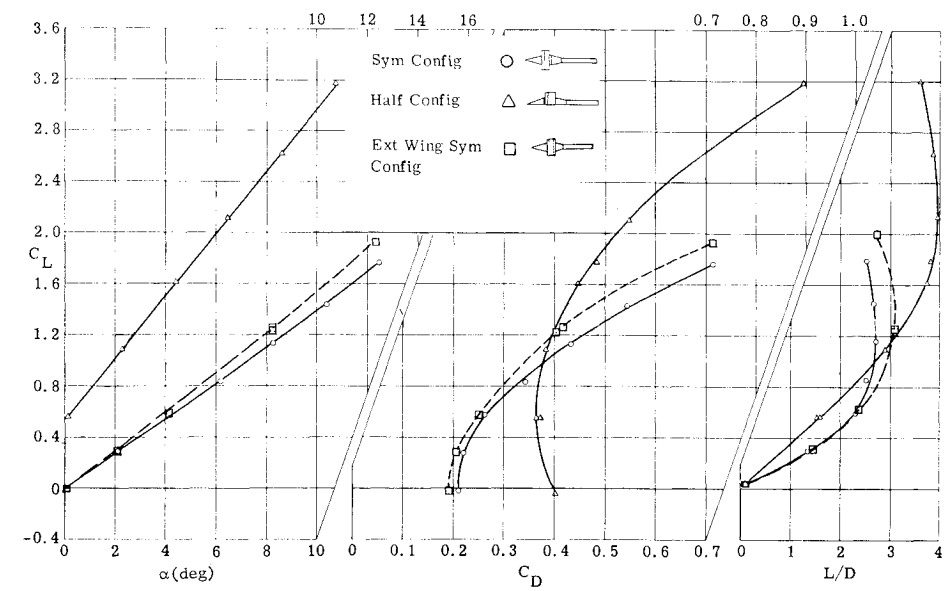

Fig. 7 A comparison of force polars of the symmetrical and unsymmetrical boattailed configurations at $M_\infty = 2.48$.

greater drag reduction is obtained with the symmetrical models than with the unsymmetric (Fig. 7). In contrast, the unsymmetrical model has a substantially greater maximum L/D; this occurs at a higher lift coefficient than for the symmetrical models.

A comparison of the variation of minimum drag $C_{D_{min}}$ with Mach number for the boattailed symmetrical and half-model configurations appears in Fig. 8. One can see that the half model is less sensitive to change in Mach number than is the symmetrical model. As a matter of fact, the half ring-wing configuration performs better at $M_\infty = 2.16$ than at the so-called design Mach number of 2.48. This is probably due, in large measure, to the fact that sufficient testing to determine an optimum minimum-drag conical boattail for the unsymmetrical model could not be conducted during this program. As the half-model boattail shape is not one that produces maximum drag reduction at a given design Mach number, the beneficial aerodynamic interference does not deteriorate as rapidly at off-design Mach numbers as does that of the symmetrical model. Insofar as the half-model interference lift is concerned, however, it should be noted that the wing location was chosen to capture the shock at a point immediately behind the leading edge at $M_\infty = 2.48$. Thus, as shown in Fig. 9, maximum interference lift $C_{L_{int}}$ is produced at approximately this Mach number.

Applications

Although a detailed discussion of the many possible applications of ring wings cannot be given here, a few comments concerning their use may be appropriate. Aside from the obvious possibilities, ring wing-body combinations probably would be particularly effective when employed, as mentioned in Ref. 4, on missions involving ballistic flight paths in the atmosphere. Ring wings also might be introduced in conjunction with auxiliary bodies or external stores noticeably to reduce their additive drag at supersonic speeds. It is also possible that they may be used advantageously in those instances where an oversize or low fineness ratio nose is required to house an antenna.

Configurations such as those sketched in Fig. 10 might prove worthwhile. In these sketches, a low drag, high fineness ratio nose is utilized with a bulging afterbody, housing for example, a powerplant or warhead. The ring wing serves to provide substantial wave drag reduction of this afterbody. Such configurations would not have the stability problem that would be associated with the use of shapes of the type tested in the present program. Futhermore, it is not difficult to visualize how, at higher Mach numbers and relatively smaller ring diameters, ring-wing bodies might form the basis of scramjet vehicles with low wave drag.

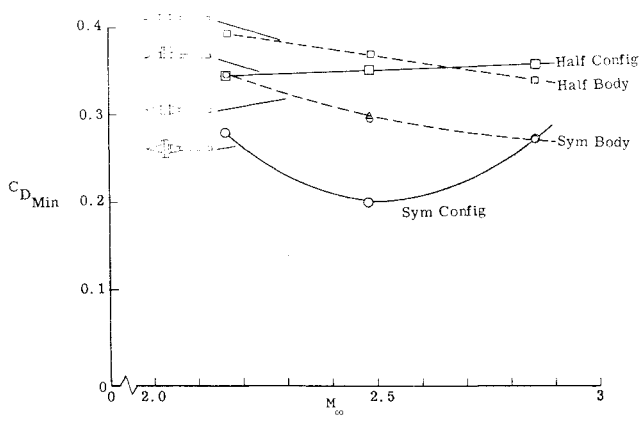

Fig. 8 Minimum-drag variation with Mach number of several boattailed symmetrical and unsymmetrical configurations.

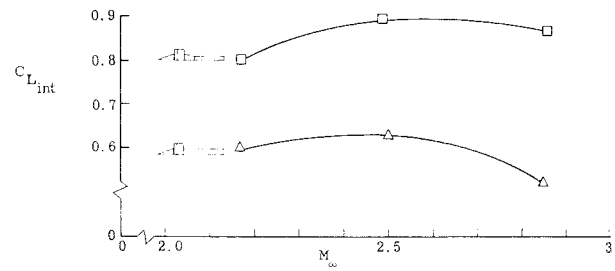

Fig. 9 Experimental interference lift variation with Mach number for the boattailed and nonboattailed half-ring-wing configuration at $\alpha = 0°$.

Conclusions

At supersonic speeds, a ring wing can be used in combination with a boattailed body to obtain significant beneficial interference effects. Tests of variations in boattail angle and location on the basic symmetrical wing-body configuration enabled us to infer an optimum geometry which had a zero-lift drag that was 33% less than that of the boattailed body alone, and 46% less than that of nonboattailed wing-body combination. This reduction is brought about largely by a reduction of approximately 88% in the wave drag of the boattailed body because of the presence of the wing. Additional experiments with the basic configuration indicate that the beneficial interference effects diminish gradually with increasing magnitude of angle of attack or as Mach number deviates from the design condition. An internal wedge extension was added to the chord of the basic ring and, when tested with the basic boattailed body, produced a zero-lift drag that was 40% lower than that of the boattailed body alone. Apparently, further work could lead to additional performance improvements.

The half-ring unsymmetrical configuration produced large interference lift that is relatively insensitive to deviations from the design Mach number. Because only a limited amount of boattailing could be used with this model, the full potential for reducing its high drag level could not be realized. In spite of its high drag, the interference lift of the unsymmetrical configuration was sufficiently large, so that the L/D of the half-ring model was much higher than that of the symmetrical configuration. Thus, it might prove fruitful to test more extensively some partial ring wings in conjunction with more efficient bodies, perhaps even symmetrical ones.§

As shown in the Appendix, the analytical method of Ref. 6 for predicting the pressure distributions on the wing and the interference pressure distributions on the body provides reasonable agreement with experiment. Efforts to predict

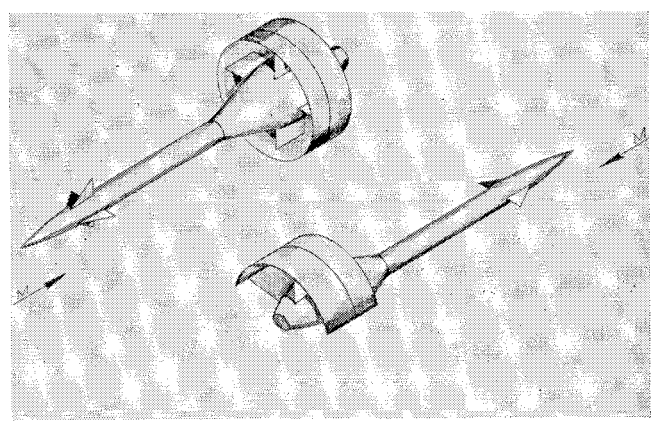

Fig. 10 Sketches of possible ring-wing configurations.

§ It recently has come to the attention of the authors that some steps in this direction have been taken by Odell Morris.[8]

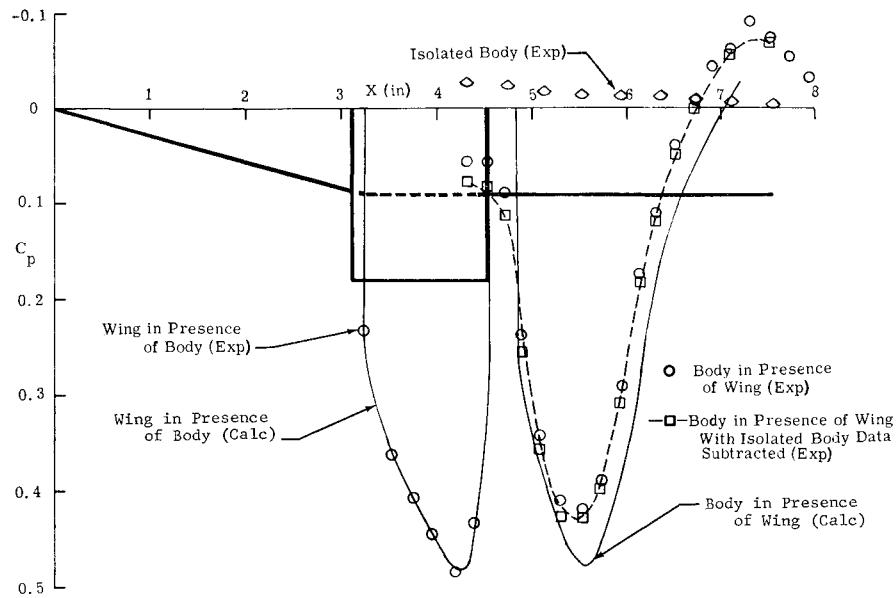

Fig. 11 Experimental and calculated pressure distributions on the wing and body of the nonboattailed symmetrical configuration at $M_\infty = 2.48$.

the optimum conical boattail location and angle for a given initial wing and nose geometry were rather successful.

Appendix: Comparisons of Experiment with Analytical Method of Ref. 6

The method of analysis used in Ref. 6 was initiated to provide guidance in the design of the symmetrical models for our experimental program. It is a semiempirical method primarily devised to provide more realistic results than those obtainable from ordinary linearized theory but it avoids the lengthy calculations required for a characteristic solution. Some comparisons with the experimental results are presented here.

Pressure Distributions

Three pressure instrumented model components were constructed: a wing model that has six static pressure orifices along the inner surface; a cylindrical body section with a longitudinal row of 10 orifices that can be rotated to any meridional location; and a 10° pressure instrumented boattail that also can be rotated. Both body elements can be positioned in various axial locations. Pressures were recorded at five circumferential stations 45° apart. However, for clarity the experimental pressure data that are presented are average circumferential values for each station. Very little difference was noted from one distribution to another.

Figure 11 contains analytical and experimental pressure distributions on the nonboattailed model at $M_\infty = 2.48$. In this figure are plotted experimental pressures measured on the wing, the isolated body, and the body in the presence of the wing with the isolated body data subtracted. Calculated interference pressures on the wing and on the body are shown also for comparison. The wing pressure distributions are in rather good agreement, but the body pressure distributions do not compare quite as well. This is especially noticeable in the region where the shock reflected by the wing intersects the body. The approximations introduced in the inviscid calculation procedure partly are responsible for the discrepancy. However, the experimental data indicate further that there is a significant effect due to the propagation of pressure upstream through the subsonic portion of the boundary layer.

Typical pressure distributions on the 10° boattail are shown in Fig. 12. The difference between the experimental and analytical pressure distributions on the boattail of a wingless

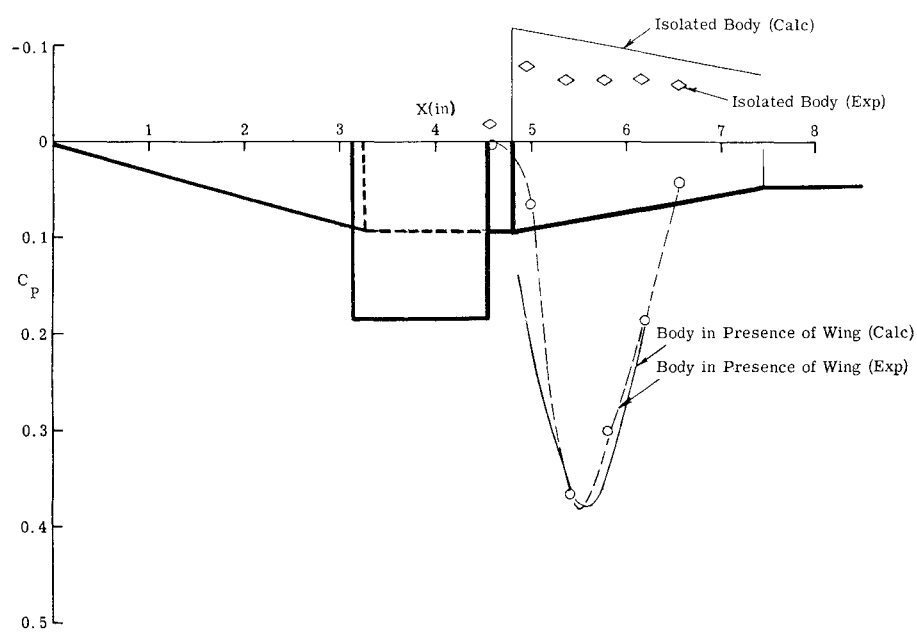

Fig. 12 Experimental and calculated pressure distributions on the 10° boattail located 4.80 in. aft of the nose of the symmetrical configuration at $M_\infty = 2.48$.

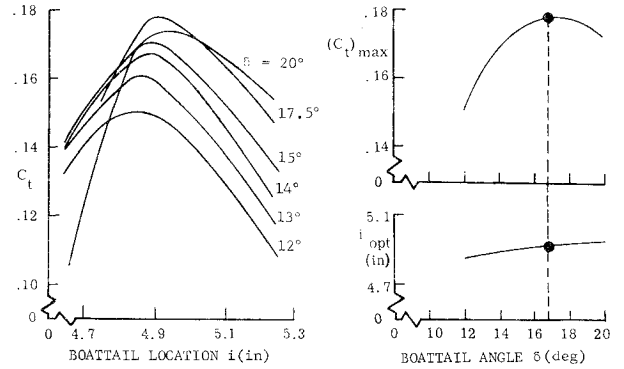

Fig. 13 Analytical determination of the geometry of the minimum-drag symmetrical configuration at $M_\infty = 2.48$.

configuration is largely due to boundary-layer separation The interference pressures resulting from the addition of the wing to the body appreciably reduce this separation.

Minimum-Drag Geometry

The net pressure force acting on the boattail is the difference between the thrust produced by the interference pressures and the wave drag of the isolated boattail. Neglecting the effects of skin friction, a boattail thrust coefficient can be defined as $C_t \equiv$ boattail interference thrust coefficient − isolated boattail wave drag coefficient. For a given nose and wing geometry and boattail base diameter, a minimum-drag conical boattail can be inferred by determining the angle and location that maximize C_t.

With the use of this technique, thrust coefficients were calculated for the family of symmetrical boattailed configurations of Fig. 1. As shown in Fig. 13, the maximizing procedure determines the minimum-drag geometry as a 16.8° boattail located 4.92 in. aft of the body nose. This compares with 13.4° and 4.91 in. obtained from the experimental results for C_{D_0} which were presented in Fig. 3. The boattail angle predicted as being best is 3.4° greater than that found experimentally. However, the curve for $(C_{D_0})_{min}$, shown in Fig. 3, indicates that this discrepancy in boattail angle corresponds to an error in minimum drag of only 3.5%.

References

[1] Ferri, A., "Application of the method of characteristics to supersonic rotational flow," NACA TR 841 (1946).

[2] Graham, E. W., Lagerstrom, P. A., Licher, R. M., and Beane, B. J., "A theoretical investigation of the drag of generalized aircraft configurations in supersonic flow," NACA TM 1421 (January 1957).

[3] Johnson, R. P., "Aerodynamic characteristics and geometric properties of half and complete ring wing configurations for supersonic design Mach number," The Rand Corp. Research Memo. RM-2208 (July 1958).

[4] Schindel, L. H., "Supersonic wind tunnel tests of ring wing configurations," Massachusetts Institute of Technology, Wright Air Development Center Tech. Rept. TR-58-220 (December 1958).

[5] Broglio, L., "Theoretical and experimental analysis of cowling configurations for the reduction of the drag on a body of revolution with large cone angle," Universita di Roma, scuola di ingegneria aeronautica, istituto di costruzioni aeronautiche, SIAR-graph 7(June 1956).

[6] Johnson, A., Mead, H., and Scheuing, R., "An experimental investigation of simple symmetric and unsymmetric supersonic ring wing configurations utilizing beneficial interference effects," Grumman Research Dept. Rept. RE-175 (May 1964); also to be made available from Defense Documentation Center.

[7] Johnson, A. and Mead, H. R., "Preliminary supersonic wind tunnel test program for ring wing body combinations at the David Taylor Model Basin," Grumman Aircraft Engineering Corp., Research Dept. Memo. RM-140, Series I–VII (September 1958–February 1961).

[8] Morris, O., "Aerodynamic characteristics in pitch of several ring-wing-body configurations at a Mach number of 2.2," NASA TN-D-1272 (April 1962).